Journal of Power Sources 270 (2014) 28–33

Contents lists available at ScienceDirect

Journal of Power Sources

journal homepage: www.elsevier.com/locate/jpowsour

High-performance tin oxide-nitrogen doped graphene aerogel hybrids as anode materials for lithium-ion batteries

Chunhui Tan [a, b, *], Jing Cao [c], Abdul Muqsit Khattak [c], Feipeng Cai [a], Bo Jiang [a], Gai Yang [a], Suqin Hu [a]

[a] Energy Research Institute of Shandong Academy of Sciences, Jinan 250014, China
[b] Key Laboratory of Colloid and Interface Chemistry, Ministry of Education, School of Chemistry and Chemical Engineering, Shandong University, Jinan 250100, China
[c] College of Chemistry and Chemical Engineering, University of Chinese Academy of Science, Beijing 100049, China

HIGHLIGHTS

- SnO_2-NGA hybrid was prepared by one-step hydrothermal method.
- The SnO_2-NGA was used as a free-standing electrode in lithium ion battery.
- The unique structure of SnO_2-NGA displays an excellent electrochemical performance.

ARTICLE INFO

Article history:
Received 11 March 2014
Received in revised form
10 July 2014
Accepted 11 July 2014
Available online 19 July 2014

Keywords:
Lithium-ion battery
Anode
Tin oxide nanoparticle
Nitrogen doped graphene aerogel
Hybrid

ABSTRACT

Tin dioxide nanoparticles on nitrogen doped graphene aerogel (SnO_2-NGA) hybrid are synthesized by one-step hydrothermal method and successfully applied in lithium-ion batteries as a free-standing anode. The electrochemical performance of SnO_2-NGA hybrid is investigated by galvanostatic charge −discharge cycling, rate capability test, cyclic voltammetry and electrochemical impedance spectroscopy. It is found that the SnO_2-NGA hybrid with freestanding spongy-like structure exhibit remarkable lithium storage capacity (1100 mAh g^{-1} after 100 cycles), good cycling stability and high rate capability. The outstanding performance is attributed to the uniform SnO_2 nanoparticles, unique spongy-like structure and N doping defect for Li^+ diffusion.

1. Introduction

Because of their high energy density, long cycle life and high security, lithium-ion batteries (LIBs) are widely utilized in portable devices and also become one of the dominant energy storage devices for hybrid electric vehicles (HEVs) and electric vehicles (EVs). However, traditional graphitic carbon material severely hinders the development of LIBs anode because of its safety issues and limited theoretical capacity (372 mAh g^{-1}) [1].

To design the novel composite materials is an efficient way to resolve the safety issues and promote its performance. SnO_2 nanomaterial is a prospective candidate to replace current anode material of LIBs for the low cost, safety and environmental benignity as well as the high theoretical capacity, which could reach 1494 mAh g^{-1} [2–9]. Besides, SnO_2 nanomaterial have better reversibility and weaker volume effect than bulk SnO_2 material, which are crucial for enhancing capacity and life of LIBs [3,8,9]. However, the conductivity and agglomeration problem of pure SnO_2 nanomaterial greatly limits its practical application in electrochemical devices [10–12]. Therefore, developing carbonaceous nanocomposite, especially graphene-based nanomaterial is regarded as the suitable strategy to solve these problems [13–17].

Graphene is often used as coating material for encapsulation of active nanomaterial. As anode material of LIBs, the theoretical capacity of graphene can reach up to 744 mAh g^{-1} with creating of Li_3C structure [18]. Chemical functionalization can also potentially introduce highly reactive regions inside graphene. Nitrogen doped graphene aerogel (NGA) is prestige than pure graphene sheet for

* Corresponding author. Energy Research Institute of Shandong Academy of Sciences, Jinan 250014, China. Tel.: +86 531 82605569; fax: +86 531 82961954.
E-mail address: tanch_85@163.com (C. Tan).

http://dx.doi.org/10.1016/j.jpowsour.2014.07.059
0378-7753/

the application in energy devices, because of its three dimensional nanostructure, large surface area and good mechanical property [19–23]. Notably, NGA with abundant defect sites has an advantage in dispersion of nanoparticles, enhancing the binding force with nanoparticles and greatly promote lithium storage ability and transportation rate of Li^+ [24]. Thus, combination of SnO_2 nanoparticles and NGA could boost the conductivity of the material, relieve aggregation problem and reduce volume expansion [25–29]. So, it is an unexceptionable choice that combination of SnO_2 nanoparticles and NGA for design a high performance anode material of LIBs.

Herein, we develop a one-step hydrothermal strategy to synthesis SnO_2 nanoparticles on nitrogen doped graphene aerogel (SnO_2-NGA) hybrid without any additional surfactant and reductant. The as prepared SnO_2-NGA hybrid are then used as a freestanding anode in LIBs. Remarkably, LIBs equipped with this freestanding anode show a high specific capacity, cycling stability and rate capability during electrochemical test, which may attributes to well-dispersed SnO_2 nanoparticles, unique spongy-like structure of nitrogen doped graphene and synergetic interaction between nitrogen doped graphene sheet and SnO_2 nanoparticles.

2. Experiment

2.1. Preparations of SnO_2-NGA compound material

The graphite oxide (GO) used in this work was produced from natural graphite flakes by a modified Hummers' method [30]. The SnO_2-NGA was synthesized by one-step hydrothermal method. Firstly, 1.5 ml concentrated ammonia water and 150 ml 2 mg ml^{-1} GO aqueous dispersions were mixed and stirring 30 min sufficiently. Secondly, 0.8 g $SnCl_4 \cdot 5H_2O$ was dissolved in this mixed solution. After ultrasonic disperse for 1 h, the solution was transferred into hydrothermal reaction vessel and kept at 180 °C for 12 h for formation of hydrogels. After the products were dialyzed with ultrapure water for one day at least, they were subjected to freeze-drying at −53 °C and −30 Pa for 12 h to generate 3D SnO_2-NGA. The freeze-drying process is as following: First, the dialyzed products were put into a freeze-drying flask and kept at −20 °C in a refrigerator for 4 h. The frozen samples were subsequently transferred into a freeze-drying vessel (Model: FD-1A-50, Bo yi kang experimental instrument co., LTD, China) which had been set at the temperature of −53 °C and vacuum pressure of −30 Pa. The samples were freeze dried for at least 12 h to remove the solvent and the water phase completely. The aerogels products were stored in a vacuum desiccator at room temperature for storage and further removal of any residual solvent until being used for characterization.

The SnO_2 nanoparticle on graphene aerogel (SnO_2-GA) was synthesized by the same method without adding concentrated ammonia. The NGA was synthesized by the same method without adding $SnCl_4 \cdot 5H_2O$. The GA was synthesized by the same method without adding concentrated ammonia and $SnCl_4 \cdot 5H_2O$.

2.2. Structure analysis

The crystallographic information of the sample was recorded using a D8 Advance X-ray diffractometer (XRD, Bruker, Germany) with Cu Kα radiation in the range from 20°to 80°. The morphology of sample was observed using a JSM-7600F field emission scanning electron microscope (SEM, JEOL, Japan) and JEM-1011 transmission electron microscopy (TEM, INCAx-sight, Oxford). The element composition of the sample was analyzed by energy dispersive X-ray spectroscopy (EDX, INCAx-sight, Oxford). The graphene content in the sample was determined using a TGA/DTA SDTQ600 simultaneous thermo-gravimetric analyzer (TGA, TA, USA) in air at 10 °C min^{-1} ranging from room temperature to 800 °C. The Raman measurement of as-synthesized material was conducted on a confocal Micro Raman Spectrometer with LabRAM HR800 system (HORIBA, Korea) in the range of 1100–2000 cm^{-1}. X-ray photoelectron spectroscoy (XPS) measurements were carried out with an ESCALAB 250 spectrometer (Thermo Fisher Scientific, USA) using a twin-anode Mg/Al Kα X-ray source. Fourier Transform infrared spectroscopy of sample was recorded by Vertex 70 infrared spectrometer (FTIR, Bruker, Germany) with in the range from 600 cm^{-1} to 3500 cm^{-1}.

2.3. Test batteries assembling

The test CR2032 coin cells were assembled with a piece of as-synthesized material chip (thickness ca. 1 mm) serving as the working electrode and lithium sheet as the counter electrode and reference electrode in an argon-filled glove box at room temperature. The electrolyte was 1 mol L^{-1} $LiPF_6$ in a mixed solvent of ethylene carbonate/dimethyl carbonate/ethyl methyl carbonate in 1:1:1 (vol. %), provided by Beijing Institute of Chemical Reagents. The cathode and anode were separated by a Celgard 2400 membrane.

2.4. Electrochemical tests

Cyclic voltammetry (CV) was performed using a CHI604D Electrochemical workstation (CH Instrument, Shanghai, China) at a scan rate of 0.5 mV s^{-1} within the potential range of 0 V–3 V (vs. Li^+/Li). The charge and discharge cycling tests were performed using a CT2001C-001 Land battery testing system (Jinnuo, Wuhan, China) with a current density of 0.2 A g^{-1} at a cut-off voltage of 0.05 V–3 V (*vs.* Li^+/Li). The rate capability tests were performed with 0.2, 0.5, 1, 2 and 5 A g^{-1} respectively at the same voltage range. Electrochemical impedance spectroscopy (EIS) was performed on CHI604D Electrochemical workstation (CH Instrument, Shanghai, China). The frequency was set in 0.01 Hz–100 kHz with the amplitude of 5 mV.

3. Result and discussion

3.1. Characterizations of SnO_2-NGA hybrids

Fig. 1(a) displays a digital photo of the typical SnO_2-NGA aerogel hybrids. The electrode chip can be obtained by appropriate tailoring or physical pressing. Fig. 1(b) shows the SEM image of SnO_2-NGA hybrids with abundant pores and loose spongy structure, which would effectively facilitate mass transport of the anode. Importantly, the overlapping or coalescing of the flexible graphene sheets in the walls of the porous networks gives rise to the remarkable mechanical performance of the SnO_2-NGA including high strength and excellent toughness, which is curial for the anode manufacturing [10,20,31]. The elemental contents of SnO_2-NGA is certified by EDS and the result showing in Fig. 1(c) reveals that the N is successfully doped into the hybrid. The mass loading of SnO_2 is about 63.9 wt. % which was calculated by the EDS spectra and further affirmed by TGA curve (Fig. S1). Fig. 1(d) shows a TEM image of the SnO_2-NGA hybrids which has the similar morphology with SnO_2-GA (Fig. S2). A large amount of SnO_2 nanoparticles are homogeneously distributed on the nitrogen doped graphene sheets. The HRTEM image (Fig. 1(e)) shows that the crystal lattice fringes of SnO_2 nanoparticle is 0.33 nm corresponding to the (110) face of rutile SnO_2. The size of SnO_2 nanoparticles is about 5 ± 2 nm. XRD pattern of the SnO_2-NGA hybrid (Fig. 1(f)) displays several diffraction peaks, which could be indexed to the (110), (101), (200), (211),

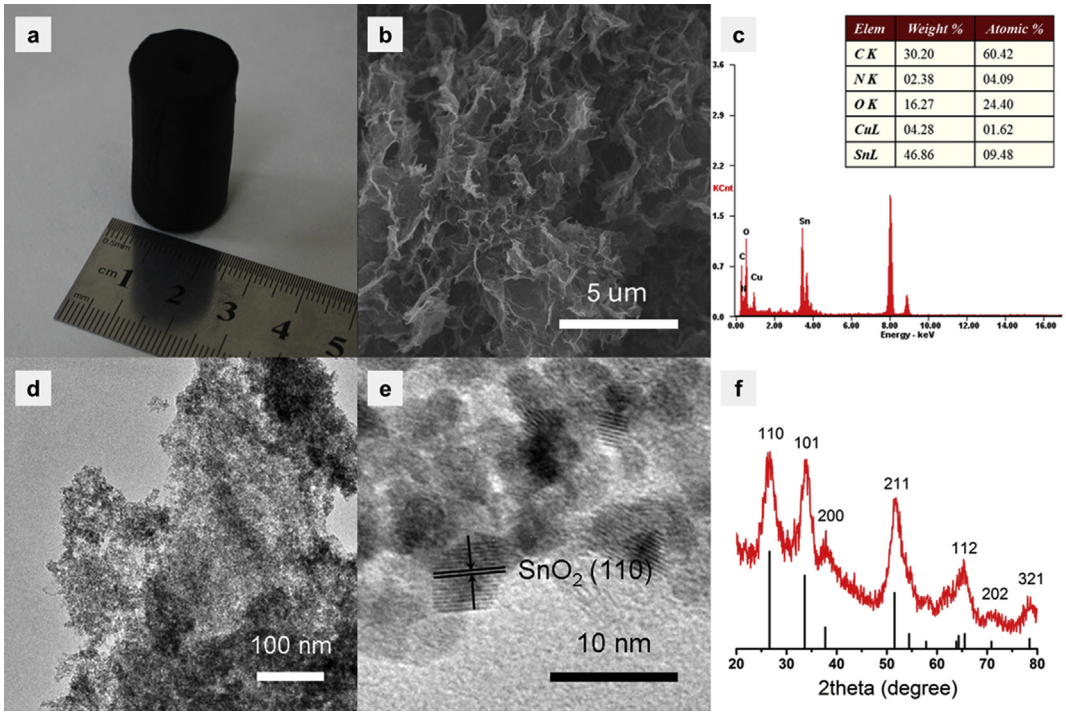

Fig. 1. (a) The photo of SnO_2-NGA aerogel column (b) The SEM image of SnO_2-NGA aerogel (c) The EDX spectrum of SnO_2-NGA hybrids (d) The TEM image of SnO_2-NGA hybrids (e) The HRTEM of SnO_2-NGA hybrids (f) XRD pattern of SnO_2-NGA hybrids and standard XRD pattern of rutile SnO_2.

(112), (202) and (321) crystal faces of rutile SnO_2 nanoparticles (JCPDS card no. 41-1445). The size of SnO_2 nanoparticle calculated by half peak width is 6.8 nm which is consist with the TEM result.

The Raman spectrums of SnO_2-NGA, SnO_2-GA and NGA are displayed in Fig. 2 for characterization the disordered carbon structure and the p-type doping effect on graphene sheet. In this figure, the intensity ratio of D band to G band (I_D/I_G) of SnO_2-NGA and NGA are 0.96 and 0.94 respectively, indicating the existence of considerable defects in graphene [32]. The defects related to disordered carbon structure, like boundaries, vacancy and amorphous structure could provide stable bonding with SnO_2 nanoparticle, active sites for lithium storage and enhanced electrochemical properties of the hybrids [33]. Nitrogen-doping brings a higher concentration of defects for the I_D/I_G of SnO_2-GA is only 0.93. The G band of the SnO_2-NGA (1597.6 cm^{-1}) has an obvious blue shift than NGA (1574.1 cm^{-1}), revealing the p-type

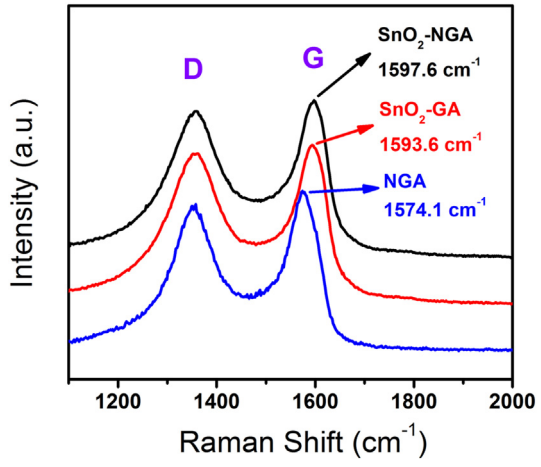

Fig. 2. The Raman spectrum of SnO_2-NGA hybrids, SnO_2-GA hybrids and NGA.

doping effect on graphene sheet (electron withdrawing effect) [34,35]. The p-type doping effect on graphene sheet discloses the electronic interactions between SnO_2 nanoparticles and graphene sheet, which facilitate the formation of desirable three-dimensional electron networks and favor electron transportation between SnO_2 and graphene sheet [33]. At the same time, G band of SnO_2-GA appears at 1593.6 cm^{-1} which means nitrogen-doping could also bring blue shift.

The chemical composition of the SnO_2-NGA is further investigated by XPS measurement. The result shows the existence of the C, O, N and Sn elements in the SnO_2-NGA hybrids (Fig. 3(a)), which is consistent with the EDS analysis result (Fig. 1(c)). Fig. 3(b) reveals that the N1s peak can be split into three peaks, which represents pyridinic-like (398.6 eV), pyrrolic-like (400.0 eV) and graphitic-type (401.4 eV) nitrogen respectively. Theoretical investigations indicates that the coexistence of vacancy and electron deficiency at the pyridinic-like defects can provide a feasible pathway for Li^+ penetration into the graphene-layers, which is beneficial for improving lithium storage properties [33,36]. As shown in Fig. 3(c), the peak of the C1s spectrum can be fitted with four types of C including C–C (284.6 eV), C–N (285.2 eV), C–O–C (epoxy groups, 286.2 eV) and O–C=O (carboxyl, 288.7 eV) can be discerned [37,38]. In Fig. 3(d), only a pair of peaks appeared at 487.5 eV and 496.0 eV are attributed to Sn 3d 5/2 and Sn 3d 3/2, which demonstrates the Sn atoms are in the form of SnO_2. The FTIR (Fig. 4) was carried out in order to confirm more information on surface functional group of nitrogen doped graphene. The FTIR spectra shows the strong peak around 1400 cm^{-1} and 3150 cm^{-1} due to C=N and N–H. The peaks appeared at 1580 m^{-1} and 1220 m^{-1} represent aromatic C=C and epoxy C–O.

3.2. Electrochemical performances of SnO_2-NGA hybrids

Fig. 5(a) shows cyclic performance of SnO_2-NGA electrode under a current density of 0.2 A g^{-1}. The initial discharge and

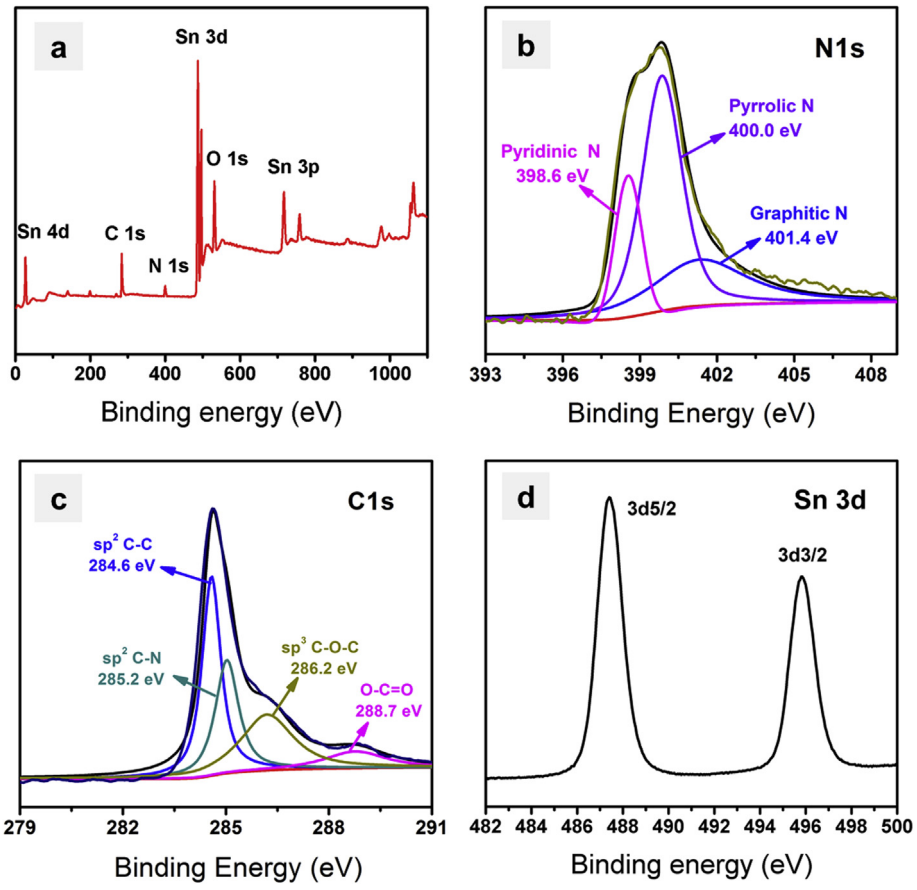

Fig. 3. (a) XPS survey scans of SnO_2-NGA hybrids (b) High-resolution XPS N 1s spectrum (c) High-resolution XPS C 1s spectrum (d) High-resolution XPS Sn 3d spectrum.

charge capacities of the SnO_2-NGA electrode are 1963 mAh g^{-1} and 1251 mAh g^{-1}. The initial columbic efficiency is only 63.7% which can be mainly ascribed to the formation of SEI and the reduction of residual oxygen-containing groups in the first cycle [39,40]. The specific capacity of SnO_2-NGA remain at 1100 mAh g^{-1} after 100 cycles corresponding to coulombic efficiency higher than 97%, showing an excellent performance and stability. It should be noted that the specific capacity values are calculated on the basis of the total mass of the SnO_2-NGA hybrid material. The cyclic performance of NGA was tested for comparison (Fig. S3). The outstanding performance can be mainly attributed to the following three reasons. As previously studies demonstrated, the first lithiation process of nano-sized SnO_2 could become reversible and the theoretical capacity reached up to 1494 mAh g^{-1}. The high specific capacity is attribute to the excellent reversibility of SnO_2-NGA, which can be further proved by CV curves. The p-type doping effect proved by Raman spectrum could strengthen electrochemical activity of SnO_2 nanoparticles and improve the reversibility of the material [33,35]. In addition, Sn—N bond or Sn—N—C bond between SnO_2 and nitrogen-doped graphene could be built in hybrids [31,41]. For that reason, there exist a stronger combination between SnO_2 nanoparticles and nitrogen-doped graphene. Thus, SnO_2-NGA exhibits a better electrochemical performance than that of SnO_2-GA (Fig. S4).

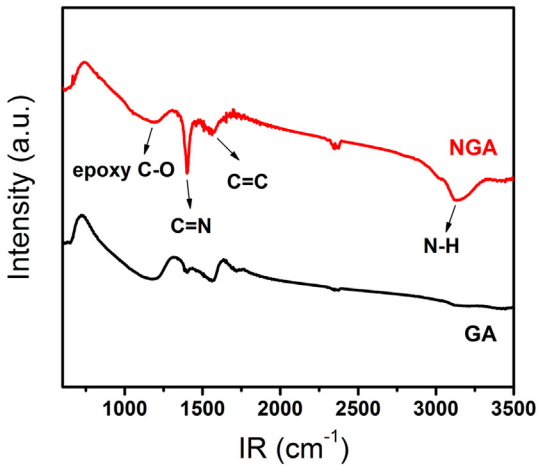

Fig. 4. The FTIR spectra of NGA (red) and GA (black). (For interpretation of the references to color in this figure legend, the reader is referred to the web version of this article.)

The charge and discharge curves of SnO_2-NGA are shown in Fig. 5(b). In these curves, two pair of platforms representing the two steps lithiation process of SnO_2. The platforms represented the first lithiation step (Eq. (1)) appeared at 1.1 V in discharge curves and 1.3 V in charge curves. Likewise, the platforms appeared at 0.3 V in discharge curves and 0.5 V in charge curves represented the second lithiation step (Eq. (2)). The two step lithiation reaction of the SnO_2-NGA hybrid exhibit good cyclic reversibility for the two couple of redox platforms have almost no change over 100 cycles.

$$SnO_2 + 4Li^+ + 4e^- \leftrightarrow 2Li_2O + Sn \quad (1)$$

$$Sn + 4.4Li^+ + 4.4e^- \leftrightarrow Li_{4.4}Sn \quad (2)$$

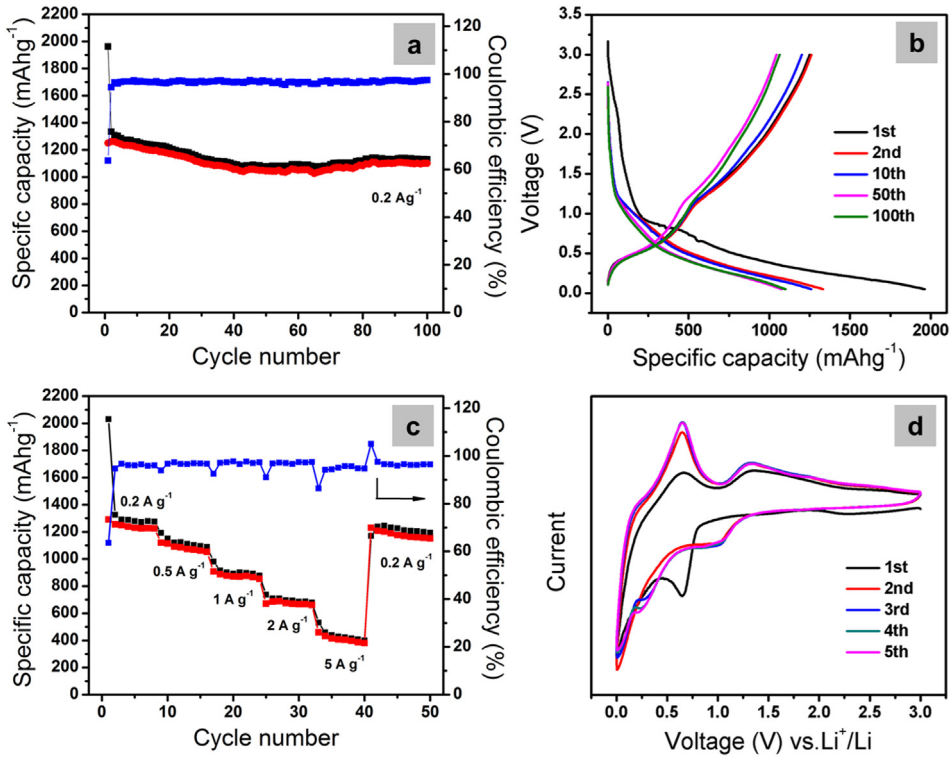

Fig. 5. (a) Cycling performance and coulombic efficiency of the SnO_2-NGA electrode (b) Galvanostatic charge/discharge curves of the initial three cycles of the SnO_2-NGA electrode (c) Rate capability of the SnO_2-NGA electrode (d) CV curves of the first five cycles of the SnO_2-NGA electrode.

The three dimensional porous nanostructure of SnO_2-NGA hybrid is beneficial for the contact between electrode and the electrolyte, and shorten the diffusion distance of Li in material. Therefore SnO_2-NGA electrode exhibits excellent rate performance as shown in Fig. 5(c). As the current densities vary from 0.2 to 0.5, 1, 2, 5 and 0.2 A g^{-1}, the average specific capacities of SnO_2-NGA electrode are 1326, 1151, 915, 709, 460 and 1203 mAh g^{-1}. Moreover, vacancy and electron deficiency existed at the pyridinic-like structure which can provide a pathway for Li penetration of the nitrogen doped graphene layer [36]. For those reason, SnO_2-NGA hybrid shows the preferable rate capacity than that of SnO_2-GA hybrid (Fig. S5). Although it decreases slightly in the higher cyclic rate but the coulumbic efficiency of SnO_2-NGA still keeps higher than 95%.

Fig. 5(d) displays the CV curves of the first five cycles of SnO_2-NGA electrode. The cathodic peak appearing at 0.7 V in the first cycle can be assigned to the decomposition of the electrolyte and formation of SEI [39,40]. From the second cycle, other two cathodic peaks appearing at 1.05 V and 0.25 V can be assigned to the formation of Li_2O and $Li_{4.4}Sn$ respectively. The corresponding anodic peaks appear at 1.30 V and 0.65 V in positive scan on behalf of the reverse reaction [8,9]. In addition, strong reduction current can be observed close to the 0 V and an oxidation peak occurs near 0.2 V in positive scan, which corresponds to lithiation and delithiation process of graphene [18]. The CV curves almost overlap except for the first cycle which implied the excellent cyclic stability. It is worthwhile to note that the regeneration of SnO_2 in oxidation process greatly increase the reversible capacity of SnO_2-NGA.

Fig. 6 shows the electrochemical impedance spectra of the SnO_2-NGA electrode before cycling, after 5 cycles, 100 cycles and the equivalent circuit model. In equivalent circuit model, the R_s and R_{ct} are resistance of the electrolyte and charge transfer respectively. Z_w is Warburg resistance and CPE is constant phase element. The resistance of the electrolyte (R_s) is 5.85 Ω before cycling. After 5 cycles and 100 cycles, this value decreased to 3.69 Ω and 3.67 Ω. The diameters of the semicircles represent the charger transfer resistances (R_{ct}) of electrochemical reaction. The charger transfer resistance of the battery before cycling was 71.3 Ω. After 5 and 100 cycles, these values become 42.6 Ω and 34.5 Ω. The significant decrease of charge transfer resistance means an enhanced electrochemical activity of SnO_2-NGA electrode.

In order to prove the influence of nitrogen-doping that brings to mass transfer of Li^+, EIS of SnO_2-GA electrode and SnO_2-NGA electrode performed in 0.5 V were used for estimate of diffusion coefficient of Li^+.

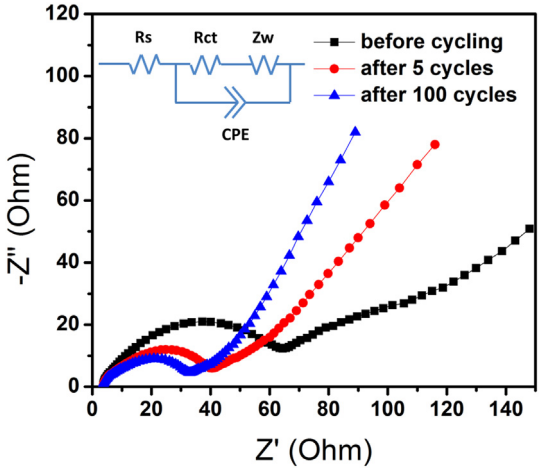

Fig. 6. The EIS of the SnO_2-NGA electrode before cycling, after 5 cycles, after 100 cycles and the equivalent circuit model (inset).

$$Z' = R_s + R_{ct} + \sigma_w \omega^{-0.5} \quad (3)$$

$$D = R^2T^2 \Big/ \left(2S^2F^4\sigma_w^2C^2\right) \quad (4)$$

The diffusion coefficient of Li^+ can be calculated from Eq. (3) and Eq. (4) in low-frequency region. Z' is the real part of impedance, ω is angular frequency, S is surface area, C is molar concentration of Li^+ ions in solid and σ_w is the Warburg factor. The estimated Li^+ ion diffusion coefficient of SnO_2-NGA and SnO_2-GA are 3.54×10^{-7} cm^2 s^{-1} and 7.84×10^{-8} cm^2 s^{-1} respectively. It is obvious that the nitrogen-doping can accelerate the transfer rate of Li ion.

4. Conclusion

One-step hydrothermal method has been developed for preparation of SnO_2-NGA hybrids material as a free-standing anode for LIBs by simple pressing. The enhanced electrochemical properties of SnO_2-NGA hybrids are proved by the electrochemistry measurements. A series of characterization and analysis indicate the high capacity, excellent electrochemical stability and outstanding rate capability attribute to the well-dispersed SnO_2 nanoparticles, the unique structure (porosity, rich defect sites, etc.) of spongy-like graphene, and the synergetic interaction between nitrogen doped graphene sheet and SnO_2 nanoparticles. Moreover, the facile and eco-friendly preparation of three dimensional SnO_2-NGA materials and electrode without need of any binders or additives is promise to be a new kind of advanced material for LIBs.

Acknowledgment

This work was financially supported by Natural Science Foundation of Shandong Province (Project No. ZR2009BM012, Project No. 2012BSC01014 and Project No. ZR2013BM023).

Appendix A. Supplementary data

Supplementary data related to this article can be found at http://dx.doi.org/10.1016/j.jpowsour.2014.07.059.

References

[1] J.M. Tarascon, M. Armand, Nature 414 (2011) 359–367.
[2] H.X. Zhang, C. Feng, Y.C. Zhai, K.L. Jiang, Q.Q. Li, S.S. Fan, Adv. Mater. 21 (2009) 2299–2304.
[3] Z. Chen, M. Zhou, Y. Cao, X. Ai, H. Yang, J. Liu, Adv. Energy Mater. 2 (2012) 95–102.
[4] M.S. Park, G.X. Wang, Y.M. Kang, D. Wexler, S.X. Dou, H.K. Liu, Angew. Chem. Int. Ed. 46 (2007) 750–753.
[5] Y. Wang, J.Y. Lee, H.C. Zeng, Chem. Mater. 17 (2005) 3899–3903.
[6] F. Wang, G. Yao, M.W. Xu, M.S. Zhao, Z.B. Sun, X.P. Song, J. Alloys Compd. 509 (2011) 5969–5973.
[7] C.D. Gu, Y.J. Mai, J.P. Zhou, Y.H. You, J.P. Tu, J. Power Sources 214 (2012) 200–207.
[8] F. Han, W.C. Li, M.R. Li, A.H. Lu, J. Mater. Chem. 22 (2012) 9645–9651.
[9] L.Y. Jiang, X.L. Wu, Y.G. Guo, L.J. Wan, J. Phys. Chem. C 113 (2009) 14213–14219.
[10] X.S. Zhou, L.J. Wan, Y.G. Guo, Adv. Mater. 25 (2013) 2152–2157.
[11] C. Kim, M. Noh, M. Choi, J. Cho, B. Park, Chem. Mater. 17 (2005) 3297–3301.
[12] N. Li, C.R. Martin, B. Scrosati, J. Power Sources 97–98 (2001) 240–243.
[13] X.W. Lou, C.M. Li, L.A. Archer, Adv. Mater. 21 (2009) 2536–2539.
[14] W.W. Zhou, J.X. Zhu, C.W. Cheng, J.P. Liu, H.P. Yang, C.X. Cong, C. Guan, X.T. Jia, H.J. Fan, Q.Y. Yan, C.M. Li, T. Yu, Energy Environ. Sci. 4 (2011) 4954–4961.
[15] Z.S. Wu, W.C. Ren, L. Wen, L.B. Gao, J.P. Zhao, Z.P. Chen, G.M. Zhou, F. Li, H.M. Cheng, ACS Nano 4 (2010) 3187–3194.
[16] S. Yang, X.L. Feng, S. Ivanovici, K. Müllen, Angew. Chem. Int. Ed. 49 (2010) 8408–8411.
[17] Q. Guo, Z. Zheng, H. Gao, J. Ma, X. Qin, J. Power Sources 240 (2013) 149–154.
[18] G.X. Wang, X.P. Shen, J. Yao, J. Park, Carbon 47 (2009) 2049–2053.
[19] Y. Xu, K. Sheng, C. Li, G. Shi, ACS Nano 4 (2010) 4324–4330.
[20] S. Zhao, H. Yin, L. Du, G. Yin, Z. Tang, S. Liu, J. Mater. Chem. A 2 (2014) 3719–3724.
[21] Z.S. Wu, A. Winter, L. Chen, Y. Sun, A. Turchanin, X. Feng, K. Müllen, Adv. Mater. 24 (2012) 5130–5135.
[22] X. Zhang, Z. Sui, B. Xu, S. Yue, Y. Luo, W. Zhan, B. Liu, J. Mater. Chem. 21 (2011) 6494–6497.
[23] W. Chen, S. Li, C. Chen, L. Yan, Adv. Mater. 23 (2011) 5679–5683.
[24] A.L.M. Reddy, A. Srivastava, S.R. Gowda, H. Gullapalli, M. Dubey, P.M. Ajayan, ACS Nano 4 (2010) 6337–6342.
[25] Y. Zhu, S. Murali, W. Cai, X. Li, J.W. Suk, J.R. Potts, R.S. Ruoff, Adv. Mater. 22 (2010) 3906–3924.
[26] X. Zhou, T. Wu, B. Hu, G. Yang, B. Han, Chem. Commun. 46 (2010) 3663–3665.
[27] S. Wang, S.P. Jiang, X. Wang, Electrochim. Acta 56 (2011) 3338–3344.
[28] C. Xu, X. Wang, J.W. Zhu, J. Phys. Chem. C 112 (2008) 19841–19845.
[29] S.M. Paek, E. Yoo, I. Honma, Nano Lett. 9 (2009) 72–75.
[30] S. Park, J. An, I. Jung, R.D. Piner, S.J. An, X. Li, A. Velamakanni, R.S. Ruoff, Nano Lett. 9 (2009) 1593–1597.
[31] Y. Liang, Y. Li, H. Wang, J. Zhou, J. Wang, T. Regier, H. Dai, Nat. Mater. 10 (2011) 780–786.
[32] G. Wang, J. Yang, J. Park, X. Gou, B. Wang, H. Liu, J. Yao, J. Phys. Chem. C 112 (2008) 8192–8195.
[33] C. Xu, J. Sun, L. Gao, Nanoscale 4 (2012) 5425–5430.
[34] C.H. Xu, J. Sun, L. Gao, J. Mater. Chem. 21 (2011) 11253–11258.
[35] B. Das, R. Voggu, C.S. Rout, C.N.R. Rao, Chem. Commun. (2008) 5155–5157.
[36] Y.F. Li, Z. Zhou, L.B. Wang, J. Chem. Phys. 129 (2008) 104703.
[37] Z. Li, Y. Mi, X. Liu, S. Liu, S. Yang, J. Wang, J. Mater. Chem. 21 (2011) 14706–14711.
[38] O.C. Compton, D.A. Dikin, K.W. Putz, L.C. Brinson, S.T. Nguyen, Adv. Mater. 22 (2010) 892–896.
[39] R. Demir-Cakan, Y.-S. Hu, M. Antonietti, J. Maier, M.-M. Titirici, Chem. Mater. 20 (2008) 1227–1229.
[40] B.Z. Jang, C. Liu, D. Neff, Z. Yu, M.C. Wang, W. Xiong, A. Zhamu, Nano Lett. 11 (2011) 3785–3791.
[41] T. Akatsuka, M. Ushiro, S.I. Nagamatsu, Y. Takahashi, T. Fujikawa, Polyhedron 27 (2008) 3146–3150.